mining

MDPI

Article

The Application of Geosynthetics in Tailings Storage Facilities: A General Review

Ronald Kerry Rowe and Jiying Fan *

GeoEngineering Centre at Queen's-RMC, Department of Civil Engineering, Queen's University, Kingston, ON K7L 3N6, Canada; kerry.rowe@queensu.ca
* Correspondence: jiying.fan@queensu.ca

Abstract: This paper is a summary of many of the key findings on the application of geosynthetics in tailings storage facilities. Topics include the compressibility and permeability of tailings, the equations predicting leakage through circular and non-circular geomembrane holes, the effect of the subgrade permeability, and the effect of a lateral drainage system within tailings on leakage predictions. Two commonly encountered engineering problems relating to the piping through circular geomembrane holes and the opening width of non-circular defective geomembrane seams are given to demonstrate the potential application of leakage prediction equations. Meanwhile, issues related to the subgrade imperfection and the long-term performance of both high-density polyethylene (HDPE) and bituminous geomembranes in tailings storage applications are addressed. The research highlights that an appropriate HDPE geomembrane liner can be expected to perform very well for an extremely long time, limiting leakage and contaminant migration from the facility into the surrounding environment if the liner is well constructed on a suitable subgrade.

Keywords: tailings; geosynthetics; geomembrane; hole; seam; leakage; erosion; tensile strain

check for updates

Citation: Rowe, R.K.; Fan, J. The Application of Geosynthetics in Tailings Storage Facilities: A General Review. *Mining* **2024**, *4*, 447–468. https://doi.org/10.3390/mining4020026

Academic Editor: Shuai Cao

Received: 6 May 2024
Revised: 3 June 2024
Accepted: 6 June 2024
Published: 15 June 2024

1. Introduction

The 2014 Mount Polley tailings dam failure was a shock to geotechnical and mining engineers. Since then, there have been other examples, including a decommissioned Brazilian iron mine dam that collapsed catastrophically in 2019, unleashing a mudflow that killed 270 people [1]. Statistical analyses have shown that the main causes of tailings dam failures from 1915 to 2016 were earthquakes, overtopping, seepage and internal erosion, slope instability, and inadequate foundation [2]. Heightened concern about dam stability has been accompanied by an increased recognition of potential environmental liabilities and more frequent use of geomembrane (GMB) liners in recent years [3–11].

GMBs underlain by a less permeable layer, such as a compacted clay liner or geosynthetic clay liner, and overlain by a highly permeable layer have proven to be very effective at minimizing environmental impacts due to landfills and contaminants of concern in the last century [10,12–24]. Unlike relatively permeable municipal solid waste (MSW), TSFs are engineered structures that are constructed to impound slurry, thickened, and paste tailings resulting from mineral extraction activities, which typically have much lower hydraulic conductivity. The MSW and the geosynthetic liner system for TSFs commonly comprise tailings directly over a single GMB liner and the subgrade despite the fact that the water head within the TSF may be greater than 100 m [5,25]. This is because tailings with typical 40–70% fines content (<75 μm) [26] can potentially form a lower permeable layer above the liner at the base of a TSF impoundment—in essence, an inverted composite liner.

GMBs used in TSF are usually either high-density (HDPE) or linear low-density (LLDPE) polyethylene with a typical thickness of 1.0 to 2.5 mm [5,8]. With a GMB liner at the base of a TSF impoundment, the leakage is effectively limited to flow through GMB defects that commonly arise either during construction or subsequently due to long-term stress cracking [10,12–17,27–33]. A geosynthetic liner leakage simulator (GLLS) was

developed by Brachman et al. (2017) [34] to study the leakage through a circular GMB hole in tailings storage applications under simulated field conditions. The GLLS was subsequently modified to expand its application to water impoundment by Fan and Rowe (2023) [35]. With the help of GLLS, many factors affecting leakage through GMB defects in a TSF were examined experimentally, numerically, and analytically by the authors. These factors have included the thickness of tailings, their properties, water head, GMB hole size and hole shape, GMB thickness, subgrade permeability, filter compatibility, and drainage.

This paper serves as a summary of recent findings relating to the application of geosynthetics in TSFs. Topics include the impact of fines within tailings on compressibility and permeability [26,36]; the development of equations predicting leakage through circular [37] and non-circular [38,39] geomembrane holes overlain by saturated tailings and underlain by a highly permeable subgrade; the effect of the subgrade's permeability [40]; and the effect of a lateral drainage system within tailings [25] on leakage. Piping and internal erosion are discussed [41], as is the opening width of defective seams [42]. Finally, issues related to the subgrade imperfection on the serviceability of GMB in TSFs (i.e., tensile strain as given in [43]) and the erosion of subgrade soil containing soluble minerals like gypsum [44] are discussed. A framework diagram describing the correlation among the various research points is given in Appendix A.

2. Mechanical Properties of Tailings

A permeameter (Figure 1) was designed to study the compressibility and permeability of tailings. It could be used to conduct one-dimensional consolidation testing using incremental loading followed by a hydraulic conductivity (k) test after each consolidation stage without causing specimen disturbance. Detailed descriptions of this apparatus are given by [36,37].

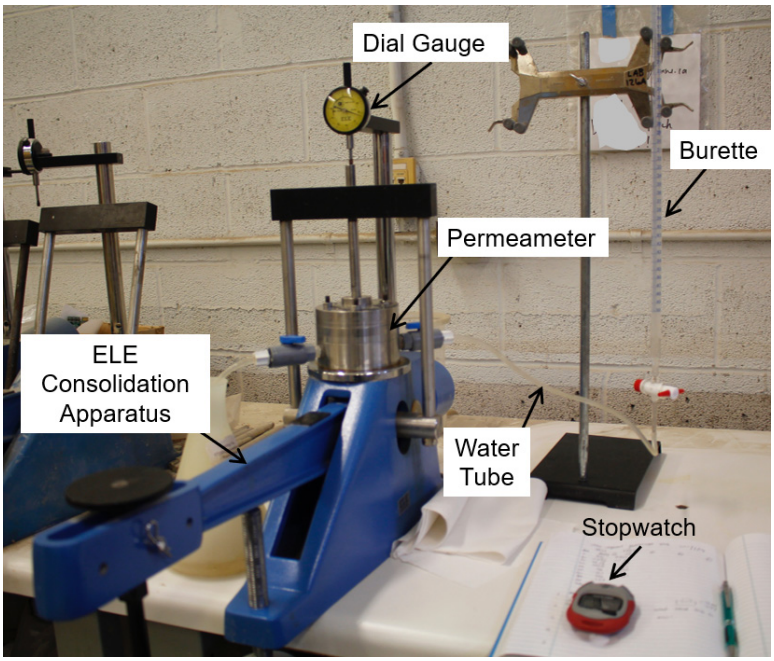

Figure 1. Stress-dependent permeameter test described by Fan et al. (2022) [36].

2.1. Compressibility

A study of the effect of the fines content of tailings on the soil skeleton and its compressibility was conducted using silty sand (SM), initially containing 18% non-plastic fines (<75 μm) and with a specific gravity of ~2.65. The diameters of the particles at which 10%, 30%, 50%, and 60% by mass were finer, denoted as d_{10}, d_{30}, d_{50}, d_{60}, respectively, were 0.035 mm, 0.12 mm, 0.18 mm, and 0.23 mm [36]. The coarse fraction of the host sand

(>75 μm) was classified as poorly graded sand (SP), with coefficients of uniformity and curvature of 2.5 and 0.8, respectively. The fine fraction of the host sand (<75 μm) had coefficients of uniformity and curvature of 15.8 and 2.8, respectively.

Sixty-five specimens with varying fines contents from 100% to 0% (by dry weight) were prepared by adding fines into or removing fines from the host sand. At the same level of consolidation stress, the test results showed that the void ratio (denoted as *e*) corresponding to 100% primary consolidation decreased notably when the fines content increased from 3% to 30%, then *e* remained constant when the fines increased from 30% to 50%, and *e* increased when the fines increased from 50% to 100% (Figure 2).

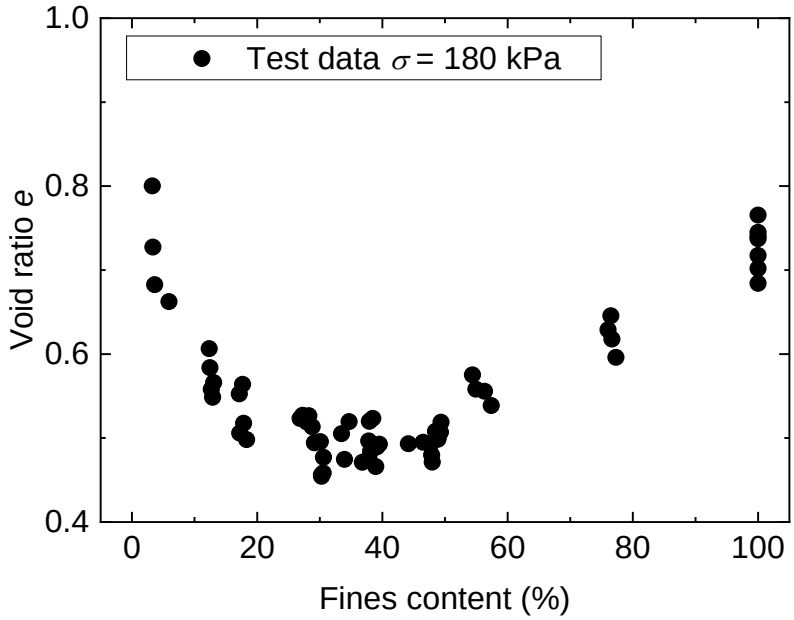

Figure 2. Variation in *e* at 100% primary consolidation versus fines content at the applied stress of 180 kPa.

The secant-confined compressibility, denoted as C_C, between two adjacent loading stages can generally be summarized as:

Phase I: fines content between 0 and 10%, fines were not involved in compression, and C_C was equal to the compressibility of the coarse fraction (denoted as $C_{Ccoarse}$).

Phase II: fines content between 10% and 35%, fines were partially involved in compression, and the percent of fines involvement increased with the increasing fines content; therefore, C_C rises in Figure 3.

Phase III: fines content between 35% and 40%, all the fines and coarse grains were involved in compression; since fines were more compressible than the coarse in this case, the cushioning effect surrounding the coarse resulted in a reduction in $C_{Ccoarse}$; the cushioning effect increased with the increasing fines content and the consequent increasing distance between the coarse particles, and C_C dropped in this phase.

Phase IV: fines content between 40% and 100%, the coarse grains were fully dispersed in the fines matrix, the cushioning effect became constant, and C_C increased linearly.

The investigation of fines involvement in the soil skeleton is critical when studying the potential for seepage-induced internal stability of cohesionless soils [45]. For the fines that are not involved in compression, fines migration may arise if the size of the fines is less than that of the constrictions. This can explain the observation of migration of fines through the GMB defect when overlain by silty sand tailings with a fines content of 25–27% by [46]. Similar fines migration was also observed from the authors' GLLS testing when the GMB was overlain by the aforementioned host sand with 18% fines content.

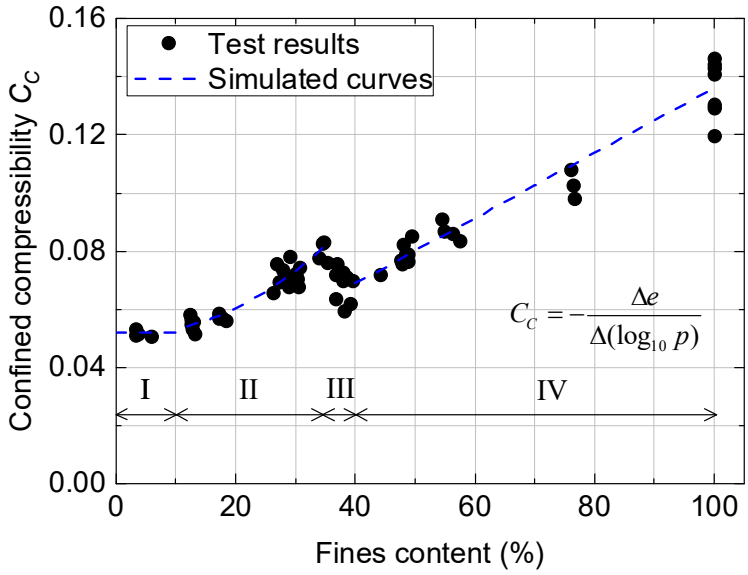

Figure 3. Secant-confined compressibility C_C versus fines content with the consolidation stress increasing from 390 kPa to 610 kPa (Note: the dashed line was the simulated curve based on Equation (3)).

2.2. Permeability

Tailings are sourced from crushing and grinding ores, and the consequent irregular shape of tailings particles results in more tortuous flow paths, changing k compared to similar-sized natural soil. The effect of fines content on the k of tailings was investigated using the stress-dependent permeameter with the same aforementioned host sand material [36]. At the same consolidation stress, the test results showed that there was an over 20-fold decrease in k as the proportion of fines increased from 12% to 40%. However, from 40 to 100% fines, there was very little further decrease in k (Figure 4).

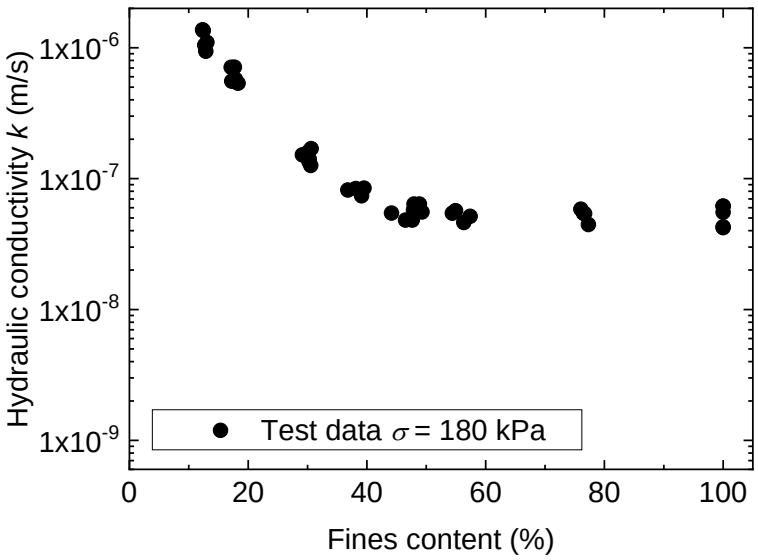

Figure 4. Variation of hydraulic conductivity k (corrected to 20 °C) versus fines content at the applied loading stress of 180 kPa.

Test results (Figure 5) from three different tailings (Table 1) with fines contents of 90% (T1; [37]), 30% (T2; [39] and 20% (T3; [41]) further confirmed the observation in Figure 4, showing that when the fines content decreased from 90% (T1) to 30% (T2), there was a ~1.5-fold increase in k, whereas there was a ~40-fold increase in k when the fines content decreased from 30% (T2) to 20% (T3; [47]).

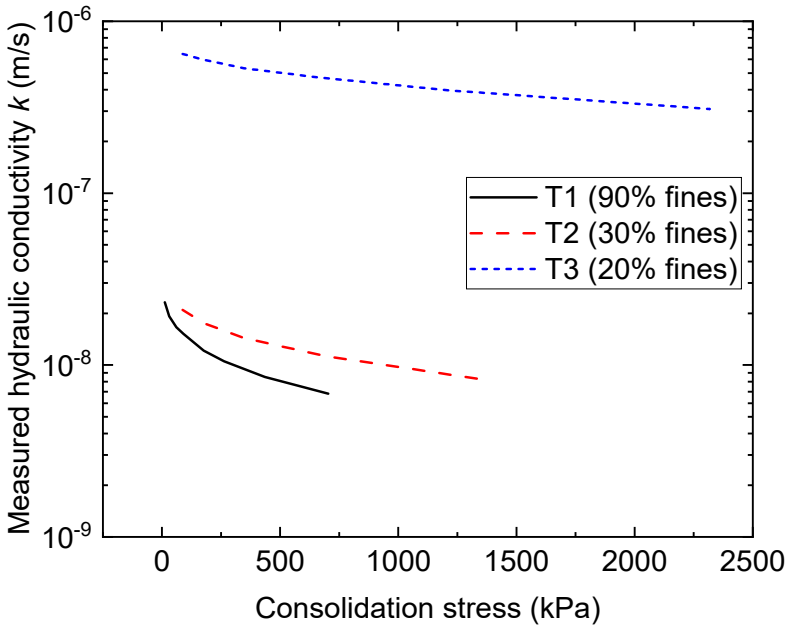

Figure 5. Measured hydraulic conductivity k of three different tailings specimens using the stress-dependent permeameter.

Table 1. Properties of tailings examined for leakage through defective GMB liners.

Tailings	Grain Size (mm)			C_u	C_c	Fines Content [a]	Specific Gravity
	d_{85}	d_{50}	d_{15}				
T1	0.07	0.01	0.002	14.3	0.9	90%	3.65
T2	0.4	0.14	0.02	23.5	3.4	30%	2.65
T3	0.4	0.18	0.06	6.2	1.4	20%	2.65

Note: [a] Percent of particles smaller than 75 µm.

Summarizing 324 experimental k values (the authors contributed 235 data points) for various tailings from previous publications, the typical size of the particle at which 10% by mass was finer, d_{10}, ranged from 0.001 mm to 0.1 mm for the summarized database, and the measured k ranged from 2×10^{-9} m/s to 2×10^{-5} m/s. According to the summarized data, an empirical equation predicting the saturated k of hard rock mine tailings when the permeant is water at 20 °C was proposed [26]:

$$k = C_u^{1/3} d_{10}^{0.38\ln(d_{10})+5.055} \left(\frac{e^3}{1+e}\right) \quad (1)$$

where k is in m/s, d_{10} is in mm, C_u is the coefficient of uniformity, and e is void ratio. Equation (1) is a modified version of the Kozeny–Carman equation [48], where the specific surface has been replaced by C_u and d_{10}, giving the best fit [26] based on a variable exponent of greater than 2 for d_{10}, emphasizing the dominant contribution of the fines to the k of tailings.

3. Prediction of Leakage through Defective GMB Lines

3.1. Circular GMB Defects

The leakage through a circular GMB hole overlain by saturated tailings with a hydraulic conductivity k_t and underlain by a permeable subgrade with a hydraulic conductivity k_s was examined theoretically and experimentally by [34,41,46,49], and in all cases with $k_s/k_t > 100$, more than 95% of the head loss occurred within the tailings in a zone up

to 5 hole diameters from the hole center; additionally, about 75% of the head loss occurred within one hole diameter from the hole center.

If the hole is filled with consolidated tailings, the ratio of head loss within the GMB hole (h_1) to the total head loss (H) can be given by (Figure 6):

$$\frac{h_1}{H} = \frac{1.42}{\frac{r}{t} + 1.42} \tag{2}$$

when the subgrade can be classified as SP (Figure 7 and Table 2) or finer.

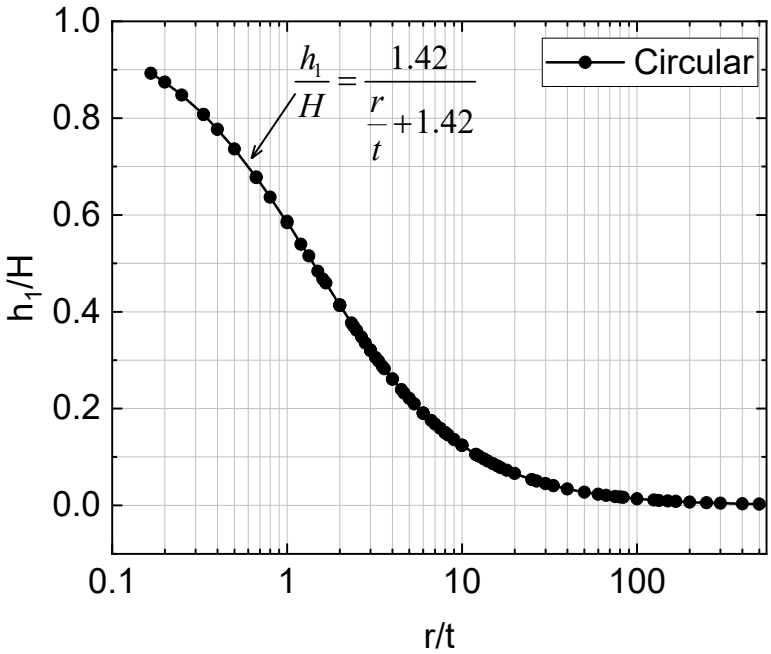

Figure 6. Head loss ratio (h_1/H) within the circular hole relative to the total head as a function of hole radius r and GMB thickness t.

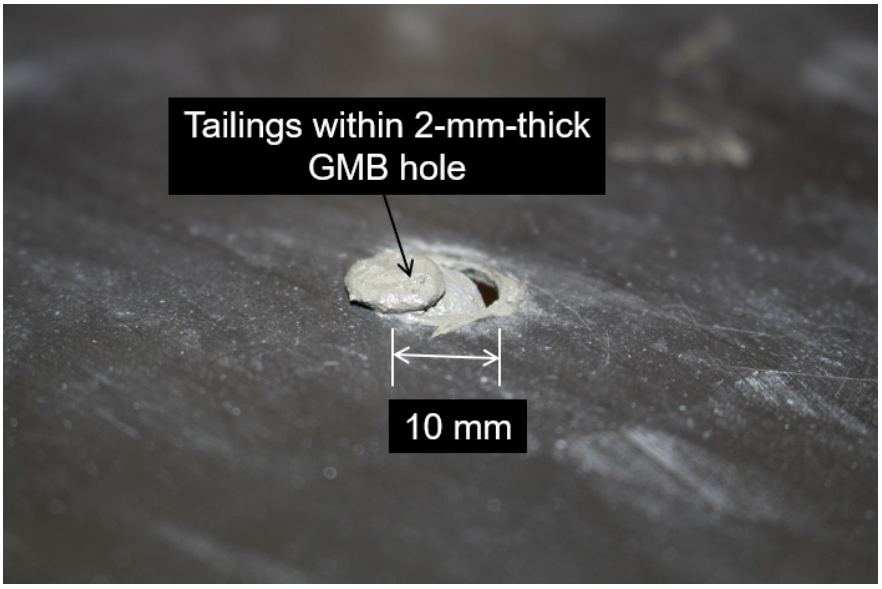

Figure 7. Post-test observation showing the consolidated T1 tailings within the 10 mm diameter hole when the GMB was underlain by SP subgrade.

Table 2. Subgrade properties for leakage through defective GMB liners.

Subgrade	Grain Size (mm)					C_u	C_c	k [a] (m/s)	Erosion Category [b] for T3 Tailings
	d_{10}	d_{15}	d_{30}	d_{60}	d_{85}				
GP	4.7	5.5	8.3	18.8	37.7	4.0	0.8	0.1	Excessive erosion
GW	2.1	3.5	8.3	18.8	37.7	8.8	1.7	0.04	Some erosion
SP	0.75	0.85	1.3	3.0	6.0	4.0	0.8	0.003	No erosion

Note: [a] Predicted using $k = 0.35\ (D_{15})^2$ ([50]). [b] Categorized based on the filtration criterion of [51].

With a coarse GP subgrade (Table 2), the intrusion of subgrade particles through the hole and the bridging of the GMB defect over a subgrade void both undermined the seepage barrier effect within the hole. Meanwhile, the spatial distribution of the fines content within tailings and the consequent homogeneity of tailings within the seepage barrier region (i.e., 5 diameters from the hole center) was proven to have a notable impact on leakage. For example, a 3% decrease in fines within 5 diameters from the hole center doubled the observed leakage [38].

The leakage through a circular hole (or a hole of any shape that can be reasonably approximated by a circle) can be obtained based on the Rowe–Booker equation [27] as follows (Case 1; Figure 8):

$$Q = \Omega_t\ \xi\ H/(\Omega_t + \xi) = \frac{H}{\frac{1}{\xi} + \frac{1}{\Omega_t}} \tag{3}$$

$$\Omega_t = \{4 + [2.455 + 0.685\ tanh\ (0.6\ ln\ (r/T))]\ r/T\}\ rk_t \tag{4}$$

$$\xi = \pi\ r^2 k_h/t \tag{5}$$

where k_h is the hydraulic conductivity of the tailings filling the GMB hole, k_t is the hydraulic conductivity of the tailing above the GMB hole, T is the thickness of the tailings, H is the total head loss within the tailings, r is the GBM hole radius, and t is the GMB thickness. If the hole is completely filled with consolidated tailings, $k_t = 1.1k_h$. This is because of the greater consolidation stress within the GMB hole relative to that above the hole.

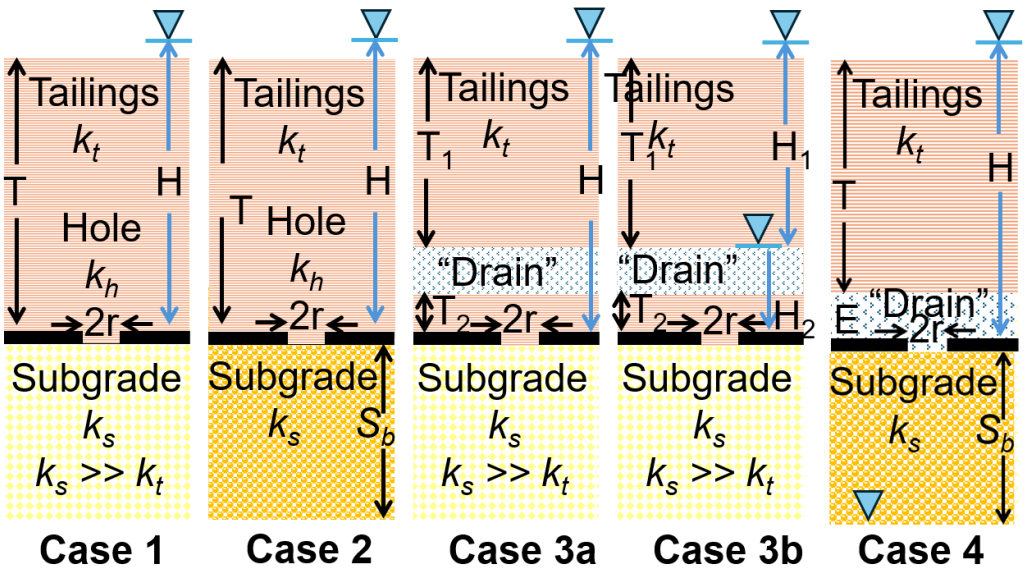

Figure 8. Leakage scenarios examined for a circular hole (radius r) in GMB. Tailings thickness, T; head, H; hydraulic conductivity above hole, k_t; hydraulic conductivity of tailings in a hole, k_h; subgrade hydraulic conductivity, k_s; subgrade thickness, S_b.

3.2. Non-Circular GMB Defects

The experimental results [38,39] showed that Equation (3) can be used for any quasi-circular hole (e.g., triangular and square) that can be approximated by a circular hole of the same area. For a rectangular hole (where B is the width and L the length) of area = $B{\cdot}L$, if the area is held constant, then the leakage increases with decreasing B/L ratio and reaches a maximum for a strip hole where $B/L \rightarrow 0$ (Figure 9). Leakage through a non-circular GMB hole overlain by saturated tailings and underlain by a highly permeable subgrade can be calculated as:

$$Q = \Lambda\, \Omega_t\, \xi\, H/(\Omega_t + \xi) \tag{6}$$

where Λ is the hole shape factor [39]. An Excel spreadsheet implementing Equation (6) was provided by [39].

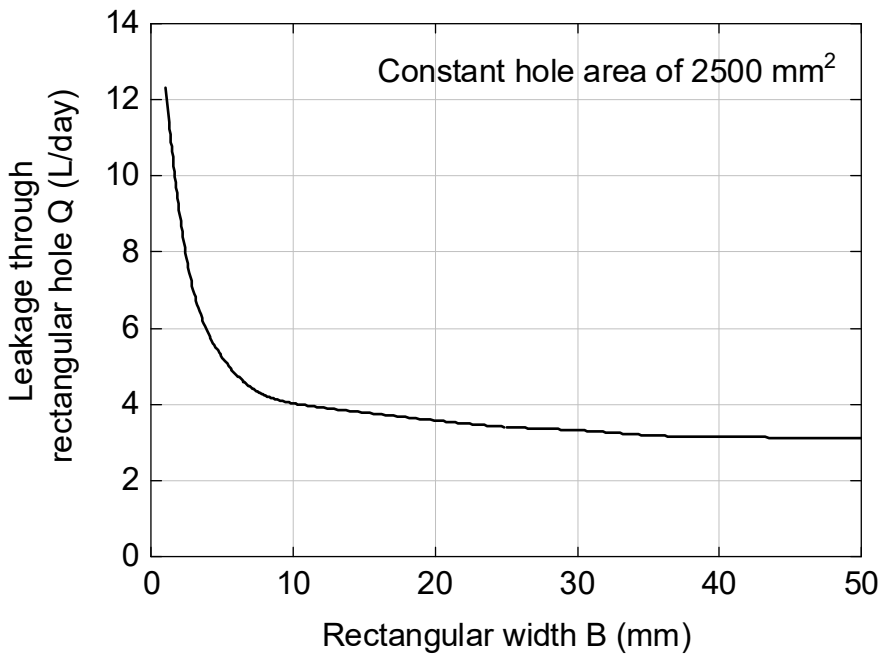

Figure 9. The variation in Q for T = 20 m, H = 21 m with a constant rectangular defect area = $L{\cdot}B$ = 2500 mm^2 (Notes: GMB thickness t is 1.5 mm, $k_1 = 1.5 \times 10^{-8}$ m/s).

3.3. Effect of Subgrade Permeability

Equations (3) and (6) both assume that the subgrade beneath the GMB is at least 100-fold more permeable than the tailings and that there is negligible head loss in the subgrade. Given the remote location and large size of a TSF, as well as the high fines content and the resulting low k of tailings, these assumptions are often appropriate. A coarse (e.g., gravelly) subgrade not only increases leakage, but also induces tensile strains in the GMB that can ultimately become the locations of stress cracks. In these situations, placement of a less aggressive cyclone silty sand subgrade beneath a GMB can reduce the maximum GMB tensile strain to less than 2% when the pressure above the GMB is increased up to 2000 kPa [43]. Leakage through any circular GMB hole in this case can be predicted by assuming Darcy's equation for leakage through the hole and the Rowe–Booker equation for leakage both above and below the GMB, as summarized by [40] (Case 2; Figure 8):

$$Q = \frac{H}{\frac{1}{\xi} + \frac{1}{\Omega_t} + \frac{1}{\Omega_s}} \tag{7}$$

$$\Omega_s = \left\{4 + \left[2.455 + 0.685 tanh\left(0.6 ln\left(\frac{r}{S_b}\right)\right)\right]\frac{r}{S_b}\right\} r k_s \tag{8}$$

where Ω_t, ξ are defined by Equations (4) and (5); k_s is the hydraulic conductivity; and S_b is the thickness of the subgrade below the GMB (Figure 8 Case 2). All other terms are as previously defined. Applications of Equation (7) showed that the leakage was notably affected by the ratio of hydraulic conductivity of the subgrade, k_s, to that of the tailings above the subgrade, k_t.

When the ratio $k_s/k_t \geq 100$, there was no significant head loss within the subgrade, leakage was unaffected by the subgrade conditions, and Equation (7) reduced to Equation (3).

When $k_s/k_t \leq 0.01$, almost all the head loss was in the subgrade, leakage was largely unaffected by tailings above the hole, and Equation (7) reduced to Equation (9) or (10):

$$Q = \frac{H}{\frac{1}{\xi} + \frac{1}{\Omega_s}} \tag{9}$$

or, if $k_h >> k_s$:

$$Q = \frac{H}{\frac{1}{\Omega_s}} = H\Omega_s \tag{10}$$

3.4. Effect of a Lateral Drainage System

Fine tailings, with a high initial water content and low k, consolidate very slowly [52]. A drainage system may be installed in a TSF to accelerate the consolidation of tailings and reduce liquefaction potential. The effects of a lateral drainage layer on leakage through a defect in a geomembrane overlain by saturated tailings were explored experimentally, numerically, and analytically by [25]. Two different positions of the internal drainage layer were examined: (a) the drainage layer was between two tailings layers (Case 3), or (b) the drainage layer was below the tailings and directly above the GMB (Case 4).

3.4.1. Case 3 Drainage Layer Is Not in Contact with GMB

For Case 3a (Figure 8), leakage through a circular GMB hole occurred when a drainage layer existed between two tailings layers, with the thickness of the tailings above the drain being T_1 (m) and k_{t1} (m/s) and the thickness being T_2 (m), k_{t2} (m/s). Assuming that the drain is permeable enough to equalize the head in that layer, but does not drain a significant amount of fluid, then the leakage through the hole can be deduced from the continuity of flow, given by [25]:

$$Q = \frac{H}{\frac{1}{\xi} + \frac{1}{\Omega_{t2}} + \frac{1}{\chi}} \tag{11}$$

$$\Omega_{t2} = \left\{4 + \left[2.455 + 0.685 tanh\left(0.6 ln\left(\frac{r}{T_2}\right)\right)\right]\frac{r}{T_2}\right\} r k_{t2} \tag{12}$$

$$\chi = A\, k_{t1}/T_1 \tag{13}$$

where A is the area of the tailings domain within which the fluid seeps through the GMB hole, i.e., 10,000/N (m^2), where N is the number of holes in the GMB per hectare if Q is the leakage (m^3/s/hole-per-hectare).

Case 3b (Figure 8) also involved leakage through a circular GMB hole when a drainage layer existed between two tailings layers, with the thickness of the tailings above the drain being T_1 (m) and k_{t1} (m/s) and the thickness being T_2 (m), k_{t2} (m/s), but in this case, the collecting fluid was commensurate with the head, H_2, in the drainage layer relative to the top of the GMB. In this case, the leakage through the hole is given by:

$$Q_h = \Omega_{t2}\, \xi\, H_2/(\Omega_{t2} + \xi) \tag{14}$$

$$\Omega_{t2} = \{4 + [2.455 + 0.685\, tanh(0.6\, ln\, (r/T_2))]\, r/T_2\}\, r k_{t2} \tag{15}$$

and ξ is given by Equation (4). The flow collected by the drain, in this case, is given by:

$$Q_{drain} = \chi\, H_1 - Q_h \geq 0 \tag{16}$$

where χ is given by Equation (13). Q_h is given by Equation (14). Q_{drain} is the drainage from an area A of the tailings domain within which the fluid seeps through the GMB hole, i.e., 10,000/N (m^2), where N is the number of holes in the GMB per hectare and Q_h is the leakage (m^3/s/hole-per-hectare) through the hole. $H = H_1 + H_2$ is the total head drop.

3.4.2. Case 3 Drainage Layer Is in Contact with GMB

Leakage through a circular GMB hole when a drainage layer, which had thickness E and hydraulic conductivity k_d, was below the tailings and directly above the GMB (Case 4; Figure 8) can be summarized as [25]:

$$Q = \frac{H + S_b}{\frac{1}{\kappa} + \frac{1}{\xi} + \frac{1}{\Omega_s}} \tag{17}$$

$$\kappa = 2\pi\theta / K_o \left[r/(\theta\, T/k_t)^{0.5}\right] \tag{18}$$

where θ is the transmissivity of the drainage layer $\theta = k_d \times E$, K_o is the zero-order modified Bessel function of the second kind, ξ is given by Equation (5), and Ω_s is given by Equation (8) [25].

The analytical solutions show that a drainage layer between two tailings layers (Case 3) results in slightly higher leakage than the scenario where no drainage layer is present, but orders of magnitude less leakage than the case where the drainage layer is directly placed above the GMB (Case 4).

4. Application of Leakage Prediction Equations

4.1. Circular Hole: Piping and Internal Erosion

Piping and internal erosion are a significant cause of failure affecting embankment dams. Monitoring leakage, both visually and quantitatively (for turbidity and changes in flow rate), is key to detecting piping and internal erosion [51,53]. An experimental program was utilized to examine how the piping of silty sand tailings was affected by the head, consolidation stress, size of the hole in the GMB, and the filter compatibility of the subgrade soil or geotextile [41,49]. The tested tailings contained 20% non-plastic fines (T3 in Table 1) and, based on the Kenney and Lau [45] criteria, were internally stable. The examined subgrades (Table 2) ranged from well-graded gravel (GW) to poorly graded sand (SP) to poorly graded gravel (GP). The applied pore pressures above the GMB were 350, 700, and 1400 kPa, respectively, with corresponding hydrostatic effective stress levels of 150, 300, and 600 kPa. The test results show that, with a filter compatible subgrade (e.g., SP, GW or GP overlain by a 450 g/m^2 GTX layer with an apparent opening size of 0.15 mm), piping did not occur, and the measured leakage correlated well with the predicted leakage using Equation (3). However, with a filter-incompatible GP subgrade, at relatively low consolidation stress when the hole diameter was 10 mm and at all the loading conditions when the hole diameter was 50 mm, the leakage was abnormally high relative to that predicted using Equation (6) (Figure 10; [41]).

The fluctuation of flow in Figure 10 for a 10 mm diameter hole was due to the development and then the collapse of the arching structure around the GMB hole, but at low-stress conditions, this was insufficient to bridge the open voids. Therefore, the fluctuating leakage in Figure 10 was hypothesized to be the consequence of periodical collapsing of an arching-induced bridging soil structure around the hole into a piping-induced void with continuing erosion of tailings through the GMB hole into the subgrade.

For the experiments in which piping did not occur, post-test exhumation showed that the migration of tailings into the subgrade through the GMB hole was notably less than that for the experiments in which piping arose (Figure 11a–e).

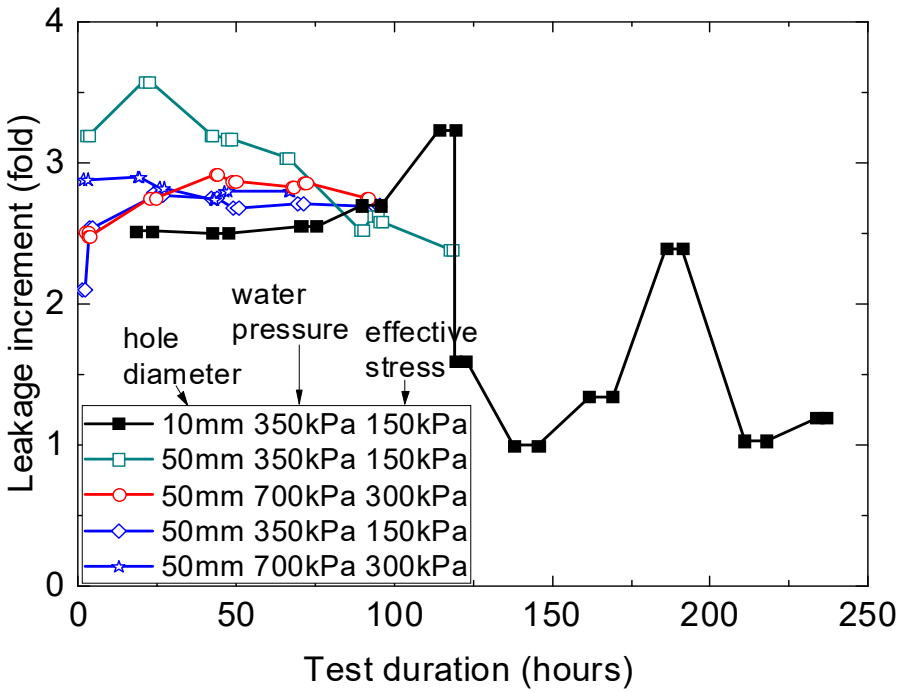

Figure 10. Leakage increment relative to the predicted leakage using proposed Equations (6) and (7) versus test duration for the piping tests with GP subgrade.

Ensuring a filter-compatible subgrade, or, if that is not possible, the use of a suitable geotextile filter (Figure 11f) between the subgrade and the GMB, is critical to the prevention of internal erosion and piping of tailings through a GMB defect. Where possible (and there are cases where this is not an option), lowering the water level increases effective stress, reduces void ratio, and thus increases resistance to piping while also reducing the driving force for piping.

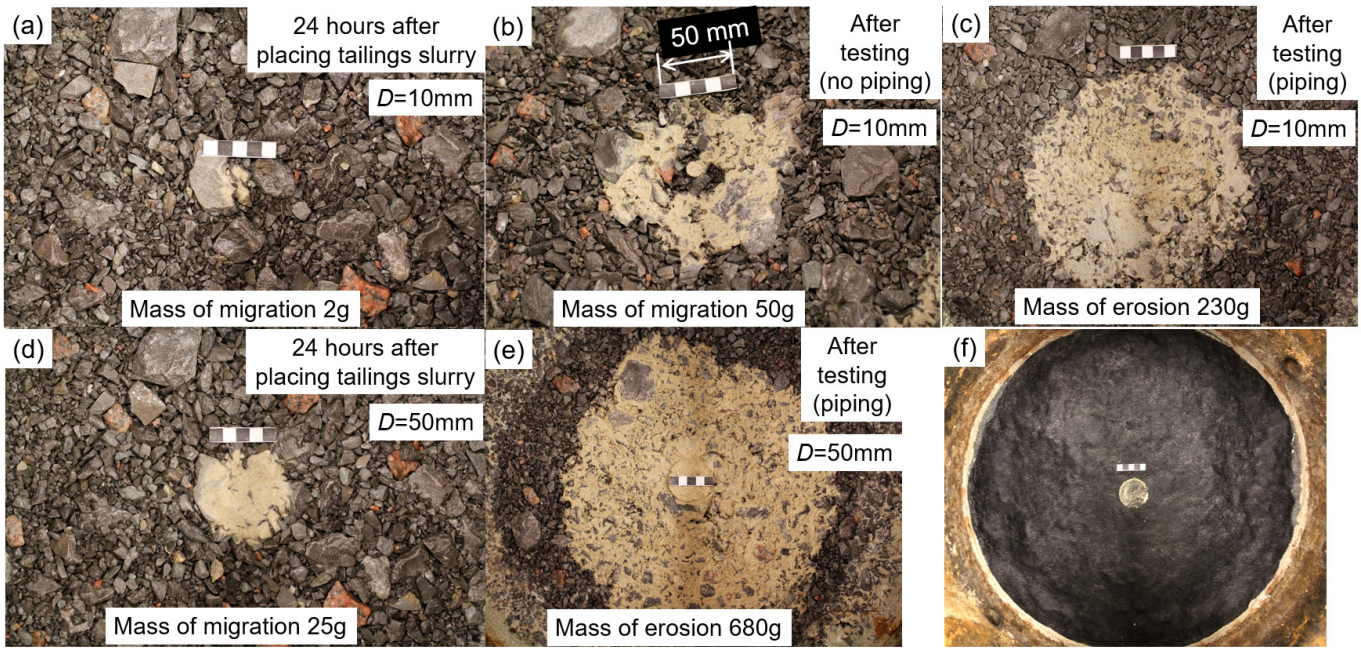

Figure 11. Post-test observations showing: (**a**) migration of tailings slurry through a 10 mm diameter GMB hole into the GP subgrade after 24 h sub-aqueous deposition; (**b**) migration of tailings into the

GP subgrade surface while placing the tailings slurry and while loading when the soil skeleton had not completely formed, with a GMB hole diameter of 10 mm; (**c**) erosion of tailings through the GMB defect into the GP subgrade, with a GMB hole diameter of 10 mm; (**d**) migration of tailings slurry through a 50 mm diameter GMB hole into the GP subgrade after 24 h sub-aqueous deposition; (**e**) erosion of tailings through the GMB defect into the GP subgrade, with a GMB hole diameter of 50 mm; (**f**) piping and internal erosion were prevented with a layer of geotextile above GP subgrade (Notes: "*D*" represents GMB hole diameter; total pressure was 2000 kPa, water pressure was 1400 kPa for Figure (**b**), total pressure was 500 kPa, and water pressure was 150 kPa for Figure (**c**,**e**)).

4.2. Non-Circular Hole: Opening Width of Defective GMB Seams

Seams and welds are a predominant source of initial defects (e.g., 55% of defects in exposed GMB liners; [54,55]), and immediately following construction, the presence of detectable leaks is between about 60- and 100-fold higher for the extrusion weld than the fusion welds per unit length of the seam [56]. Once the liner is in service, seams remain particularly vulnerable because of changes in the materials adjacent to the weld (e.g., in the heat-affected zone; [6,28,30,31,57–59] and magnification of tensile stresses [60,61]. By simplifying the cut or seam defect as a rectangular hole, the effect of subgrade on leakage through a defective GMB seam and the equivalent opening width of a defective seam can be investigated based on Equation (6). The leakage through either a knife cut slit defect (initial unstressed width $\leq$ 0.01 mm) or a defective extrusion seam overlain by saturated tailings (T2 tailings in Table 1) was measured for a range of cases, and was about 0.9 L/Day/m-head/m-defect on a GP subgrade, 0.65 L/Day/m-head/m-defect on GW subgrade, and about 0.35 L/Day/m-head/m-defect on a SP.

With an overlying total stress between 300 and 900 kPa, the opening width in these cases increased with the coarseness of the subgrade (Figure 12; [42]), being less than 1 mm when the GMB was underlain by the SP subgrade, 1.4~2 mm underlain by the GW subgrade, and 2~5 mm underlain by the GP subgrade.

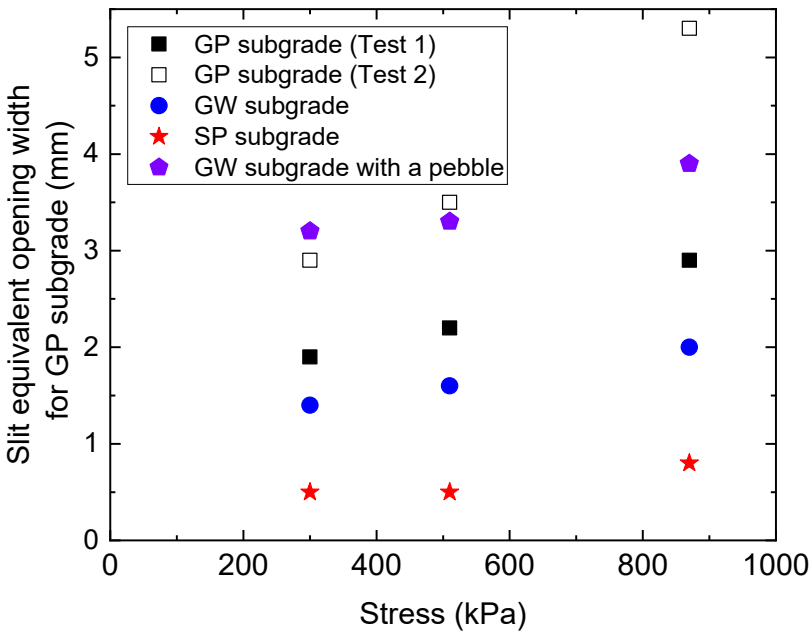

Figure 12. Comparison of the back-calculated slit/seam equivalent opening width, based on the measured leakage and the general solution predicting leakage through a GMB defect with various hole types by Rowe and Fan (2022) [39] for three different subgrades (Notes: the slit/seam defect was simplified to be a rectangular hole with the fully consolidated tailings in the hole; for GW subgrade with a pebble, a rounded pebble (15.6 mm $\times$ 23.5 mm in plan view and protruding 9.7 mm above the subgrade surface) was placed beneath the slit).

For a defective extrusion seam which was examined, leakage and the inferred equivalent opening width were substantially less critical than through a cut or stress crack with a similar length under similar subgrade and stress conditions.

5. Issues Relating to Subgrade Imperfection

Subgrade imperfection (e.g., clay desiccation cracks [62,63]) and the consequent greater interface flow through the GMB defect [16] is one of the key factors promoting the placement of a geosynthetic clay liner over a compacted clay liner beneath a GMB in municipal solid waste landfills [10,17]. The footprint of a TSF may commonly be hundreds of hectares, and a sound-engineered subgrade may not exist onsite without significant investments and earthworks. Thus, there is an incentive to explore the issues that may be encountered in a TSF relating to subgrade imperfections.

5.1. The Development of GMB Tensile Strains

The long-term serviceability of a GMB liner is directly related to the number and magnitude of local tensile strains in the GMB related to indentations from underlying or overlying materials [6,8,10,29,33,64,65]. Experiments by Fan and Rowe (2023) [43] were performed to investigate the short-term tensile strains induced in a 1.5 mm thick HDPE GMB overlain by T2 tailings (Table 1). No puncture of GMB was observed at a pressure level up to 2000 kPa. However, indentations in the GMB from the subgrade at 2000 kPa gave rise to tensile strains up to 32% for GP, 16% for GW, and 13% for SP, and no discernable indentation was observed for SM prepared at its optimum water content (11%; Figure 13).

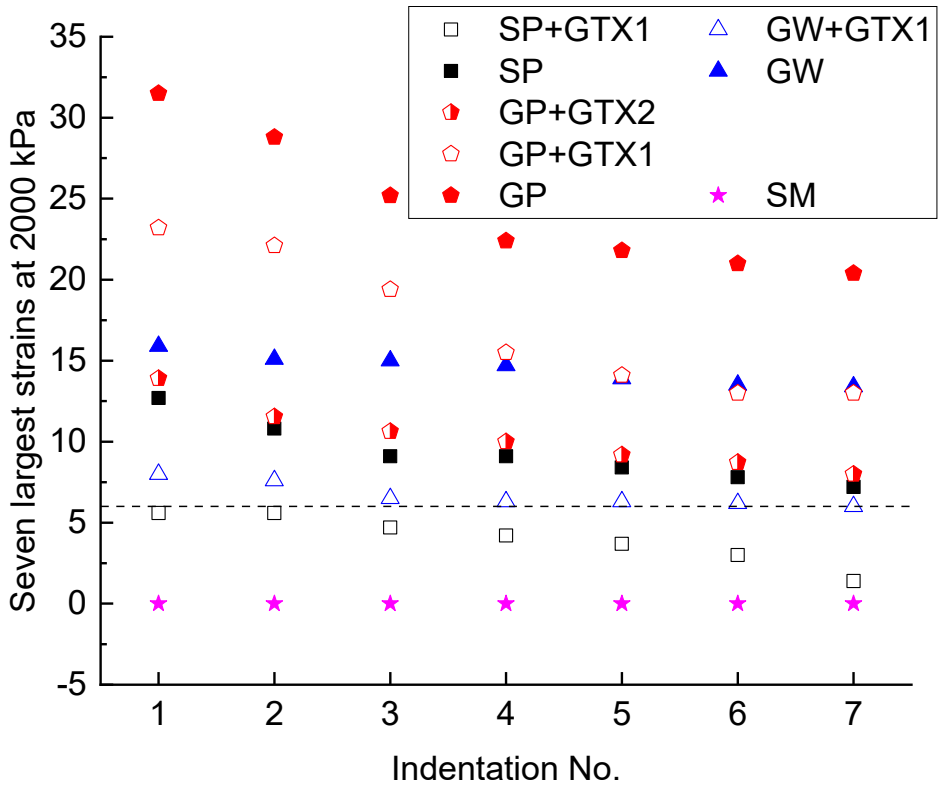

Figure 13. Seven largest strains calculated from each test, showing the effect of subgrade and geotextile protection layer on GMB strain at 2000 kPa (Notes: dashed line represents strain of 6%; GTX1 has a mass per unit area of 450 g/m^2; GTX2 has a mass per unit area of 1420 g/m^2).

The research further emphasizes the importance of a fine and even subgrade for minimizing long-term leakage by avoiding significant tensile strain (≥5%) in the GMB [10,66].

5.2. Soluble Subgrade

Soluble subgrades (e.g., gypsum $CaSO_4 \cdot 2H_2O$ and limestone) are widespread (e.g., in Europe, Australia; UK, Middle East, USA; China, and Africa). Leakage through gypsum–karst subgrades has either compromised or resulted in the catastrophic failure of many impoundment facilities (e.g., Horsetooth and Carter Lake Dams in Colorado, Upper Mangum Dam in Oklahoma, Quail Creek Dike in southwest Utah, and the Anchor Dam in Wyoming, Piney Point 2022).

Fan and Rowe (2023) [44] found that the solubility of gypsum was significant, but that the dissolution rate in contact with different solvents was extremely slow under static conditions. However, if even a small flow path existed, it was found that the rate of dissolution and erosion would increase rapidly (Figure 14). The findings from this study highlight the possible risk of having a soluble subgrade beneath a single GMB liner.

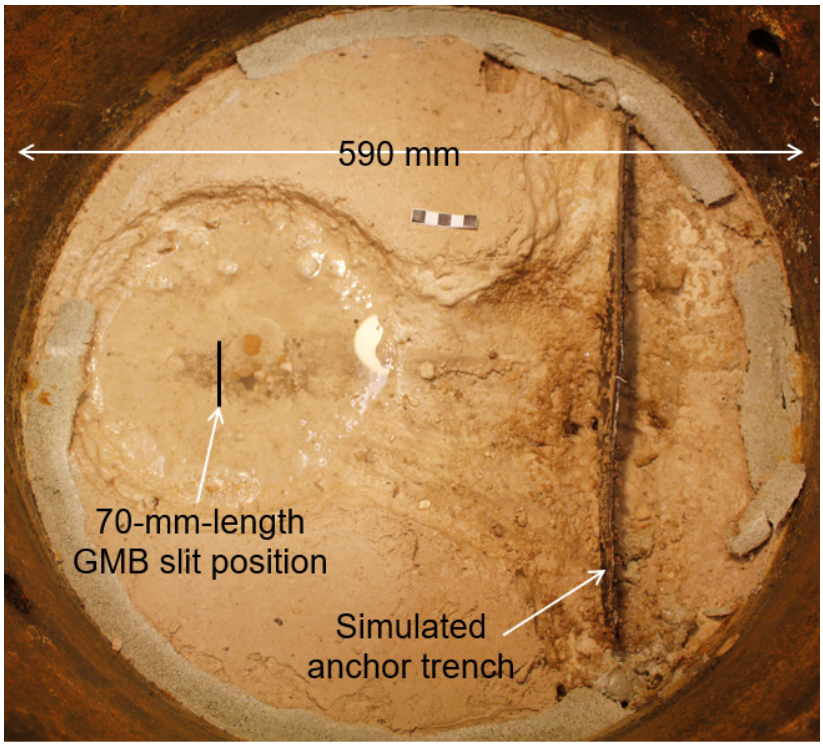

Figure 14. Effect of a soluble subgrade on leakage through a knife-cut GBM defect or a defective seam (Notes: the subgrade was rich in soluble gypsum; the solubility of gypsum in tap water is ~2.4 g/L at room temperature).

6. Service Life of Geomembrane Liners

The effectiveness of the geomembrane in reducing leakage from a TSF, as demonstrated in the previous sections, begs the question of how long they will last. This question has been subject to extensive research in recent years, as summarized below. All geomembranes have strengths and weaknesses, and a critical aspect of design is understanding these strengths and weaknesses when selecting an appropriate geomembrane for a particular application. One must consider the nature of the material to be retained, with particular emphasis on its chemistry and temperature, together with the environment in which it will be installed.

6.1. Polyethylene Geomembranes

Polyethylene has been widely used because of its high chemical resistance, relative ease of installation, and low price. Once, it was simply one layer of black plastic, but today, there can be multiple layers of geomembranes with a white surface, black surface, or a conducted black surface. The geomembranes may be smooth, textured on one side, or textured on both sides. The variability arises from the use of different medium-density

polyethylene resins and blended resins, antioxidant packages, grades of carbon blacks, grades of titanium dioxide, acid neutralizers, polymer processing aids, and any other additives (see Rowe and Jefferis [11] for details). This leads to a wide range of possible products and a huge variation in service life; depending on the chemistry and temperature and combined with their compatibility to a particular geomembrane control, the service life may range from many decades to millennia.

The service life depends on many factors. The first among these is the compatibility of the geomembrane and its constituents with the fluid that it will be required to retain. A given geomembrane may be an excellent choice for one environment and a very poor choice for another environment. There is no single geomembrane that is good for all chemistries. Studies on the effect of geomembrane-chemistry interaction, with particular emphasis on pH, have been reported by [67–71]. Temperature also significantly impacts the service life, with the service life decreasing significantly as the temperature increases. There is no way of assessing the suitability of a geomembrane for a particular application from its initial properties or experience with other solutions. The only way one can assess the relative performance is by testing the geomembrane at several elevated temperatures (e.g., 85, 75, and 65 °C or 85, 70, and 55 °C as a minimum), with additional insight being gained by testing at 55 and 40 °C as well [72]. In a recent investigation to identify a suitable geomembrane for a copper mining tailings facility, of twelve geomembranes examined, only two were found to be suitable, with the service lives varying by almost two orders of magnitude. Failure to test may result in very poor performance, including failures of incorrectly specified geomembranes within a few decades of service life for a very poor choice and within 50 to 100 years for a fair choice, whereas service lives of more than one millennium are possible at temperatures around 20 °C when using a high-quality geomembrane.

The selection of a suitable geomembrane is a very important first step. It is a necessary, but not sufficient, condition for good long-term performance. Three other factors substantially affect the service life of a very good geomembrane: exposure conditions, welding, and tensile strains.

An exposed geomembrane is subject to UV radiation, elevated temperatures on sunny days (temperatures of 80 to 90 °C have been measured on some GMBs in hot climates), potential damage by nature (e.g., wind, blowing objects, ice in cold regions), and impacts from humans and animals. The service life of exposed geomembranes is, therefore, usually less than 50 to 70 years. Buried geomembranes are subject to damage during the burial process, but are then protected from many of the exposure conditions that reduce the life of exposed geomembranes. It is buried geomembranes that could have service lives lasting millennia.

There are typically more than 1500 m of fusion welding and hundreds of extrusion welds per hectare of liner placed. Welds can be as good as the sheet if this is performed very carefully. Welds that pass typical performance tests and are judged acceptable can have service lives lasting from as little as a year to many hundreds of years, and possibly millennia, depending on the quality of the welding. The three key factors affecting the quality of the welding are heat (temperature), speed, and pressure. The right combination is required, and this depends on the material that is being welded and the ambient conditions at the time of welding. The energy that is imparted is a function of the temperature of the wedge that heats the geomembrane, the length of the wedge, and the speed of the welding machine. The energy must be sufficient to provide good bonding between two sheets of material, but not sufficient to overheat the zone in the geomembrane sheet adjacent to the weld (referred to as the heat-affected zone (HAZ)). Incorrect welding can result in a reduction in the stress crack resistance of geomembrane materials by more than one order of magnitude. As a result, the service life of a weld can be as little as 1 to 20 years, purely due to damage to the material and stresses induced during the welding process. Figure 15 shows an example of a weld performed with excess energy and pressure that failed 10 years after welding.

Figure 15. A stress crack that developed 10 years after welding because of excess pressure and temperature at the time of welding.

Figure 16 shows a hole that resulted from excessive energy and pressure with extrusion welding at a junction between three sheets of geomembranes. These weld failures often occur because the welder is attempting to weld too quickly. Passing a field quality test is not sufficient to ensure good long-term performance—acceptable but poor welds often fail within 3 to 7 years of welding due to stress cracking. There is a growing body of research highlighting the importance of appropriate welding parameters for polyethylene geomembranes (e.g., Rowe and Shoaib 2017 [30], 2018 [31]; Francey and Rowe 2024 [73]; Ali and Rowe 2024 [59]).

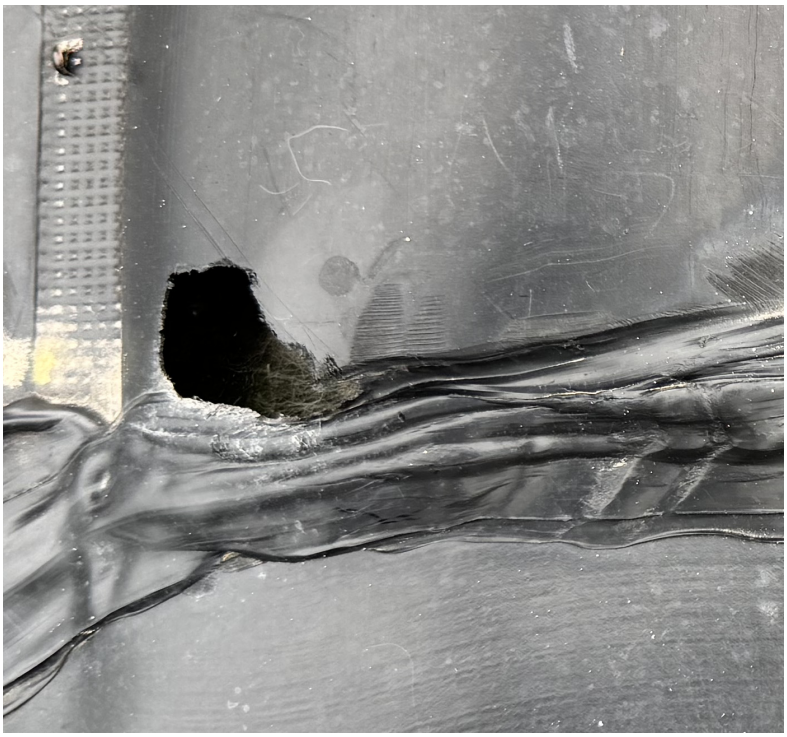

Figure 16. Hole formed 10 years after welding by stress cracking due to poor extrusion welding involving excessive temperature and pressure.

To achieve a long service life, the strain in the geomembrane should be kept below 5% and preferably below 3%. Achieving these low strains involves addressing issues discussed by [66]. It also requires a good stress crack resistance once the geomembrane reaches a stable state [74], with the value of stress crack resistance obtained after 90 days of aging at 65 °C for more than 400 h (more than 500 h is preferable).

6.2. Bituminous Geomembranes

Bituminous geomembranes have been used in some cases, both as bottom liners and as covers for mine waste. Although they are expensive, they are sold on the basis of ease of construction due to the fact that they do not wrinkle; are easy to weld; and, as is sometimes claimed, are more robust. As with polyethylene geomembranes, bituminous geomembranes (BGMs) have strengths and weaknesses.

A strength of BGMs is the fact that they do not wrinkle in the sun in the same manner as HDPE. This is a significant advantage in moderate climates. However, in hot climates, BGMs have the disadvantage of being sensitive to temperatures that can reach 70 to 90 °C in the sun, and this needs to be considered by the designer. The chemical compatibility and long-term performance of BGMs have been studied by [69,70,75–77]. Durability data based on immersion testing are shown in Table 3.

Table 3. Time to nominal failure, t_{NF} (years), of bituminous geomembranes based on immersion tests reported in the literature (lowest mechanical and chemical t_{NF}).

	Time to Nominal Failure, t_{NF} (Years), Based on Immersion Tests						
pH / Temp.	0.5	6.5 Water	9.5	11.5	Air	MSW B1	MSW B2
20 °C	100	60	55	45	70	40	31
30 °C	45	28	25	20	30	18	14
40 °C	20	15	11	10	14	8	7
55 °C	7	5	4	3	5	3	2
Ref.	#2	#1	#2	#2	#1	#3	#3

#1 Samea and Abdelaal (2023) [76]; #2 Abdelaal and Samea (2023) [69]; #3 Samea and Abdelaal (2023) [77].

A comparison of the performance with HDPE (e.g., Table 4) indicates that 1.5 mm HDPE tends to be much more chemically compatible than the 4 mm BGM (Table 4) for a given pH solution, with the difference increasing with the pH.

Table 4. Comparison of the time to nominal failure of BGMs and HDPE with immersion testing, temperature, and solution.

	Time to Nominal Failure, t_{NF} (Years), Based on Immersion Tests					
	BGM	**HDPE**	**BGM**	**HDPE**	**BGM**	**HDPE**
pH / Temp.	0.5	0.5 *	9.5	9.5 *	11.5	11.5 *
20 °C	100	>100	55	>80	45	>75
30 °C	45	>54	25	>43	20	>39
40 °C	20	>28	11	>24	10	>21
55 °C	7	>11	4	>10	3	>9
Ref.	#2	#4	#2	#5	#2	#5

* 1.5 mm HDPE times are only for antioxidant depletion; time to nominal failure is notably longer, #2 Abdelaal and Samea (2023) [69]; #4 Rowe and Abdelaal (2016) [67]; #5 Abdelaal and Rowe (2017) [68]. The HDPE considered here was selected because it has been tested for about 10 years in all three solutions. Since that geomembrane was developed early this century, better antioxidant packages have been developed and with testing for chemical compatibility, depletion times of millennia are now achievable for HDPE at 20 °C.

While BGMs seams are easy to weld, the welds have a tendency to creep to failure even if subjected to a relatively low level of tensile stress [73,78]. Regarding the issue of robustness, there is growing evidence that BGMs need as much attention as HDPE and, under the same conditions, can develop even more holes. A leak location survey at one site identified 39 holes per hectare, with dimensions up 150 mm in diameter when placed below cover soil [79].

7. Summary and Conclusions

This paper has provided a summary of many of the key findings on the application of geosynthetics in tailings storage facilities. Topics including the compressibility and permeability of tailings, the equations predicting leakage through circular and non-circular geomembrane holes, the effect of the subgrade permeability, and a lateral drainage system within tailings, along with issues related to the long-term performance of both high-density polyethylene (HDPE) and bituminous geomembranes. The proposed leakage prediction equations were used to address some engineering problems relating to piping and internal erosion and leakage with the opening width of defective seams. Finally, issues on the serviceability of geomembranes in tailings storage applications were discussed.

The research highlights that an appropriate geomembrane liner can be expected to perform very well for an extremely long time, limiting leakage and contaminant migration from the facility into the surrounding environment. The control impact can also be lowered to acceptably low levels if the appropriate liner material is selected as part of a good design and it is well constructed on a suitable subgrade. However, a suitable GMB can only be selected with immersion testing to assess its chemical compatibility with the fluid to be contained.

Author Contributions: Conceptualization, R.K.R. and J.F.; Methodology, R.K.R. and J.F.; Formal analysis, R.K.R. and J.F.; Investigation, R.K.R. and J.F.; Writing—original draft, J.F.; Writing—review & editing, R.K.R.; Funding acquisition, R.K.R. All authors have read and agreed to the published version of the manuscript.

Funding: The research reported in this paper was supported by the Natural Sciences and Engineering Research Council of Canada (NSERC) under Strategic Grant STPGP 521237–18.

Data Availability Statement: The original contributions presented in the study are included in the article, further inquiries can be directed to the corresponding author.

Acknowledgments: The tailings tested were obtained and shipped to Queen's for testing by Golder Associates and Klohn Crippen Berger. The value of discussions with Frank Barone, Roy Lopez, Harvey MacLeod, and Prabeen Joshi is gratefully acknowledged.

Conflicts of Interest: The authors declare there are no competing interests.

Appendix A

The framework diagram correlating the various research points in the manuscript.

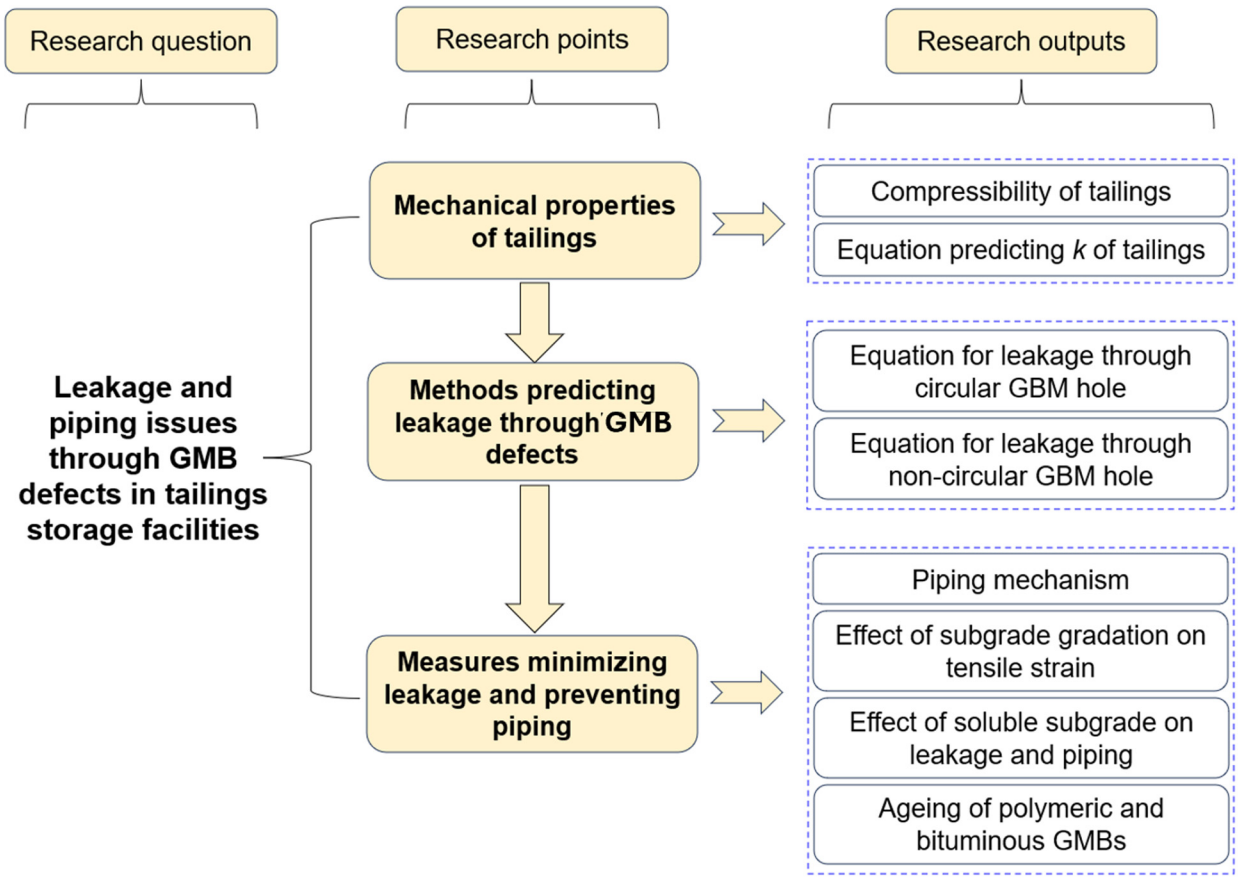

Figure A1. The framework diagram correlating the research points.

References

1. Cornwall, W. A dam big problem. *Science* **2020**, *369*, 906–909. [CrossRef] [PubMed]
2. Roche, C.; Thygesen, K.; Baker, E. Mine tailings storage: Safety is no accident. In *A UNEP Rapid Response Assessment*; United Nations Environment Programme and GRID: Arendal, Norway; Nairobi, Kenya, 2017.
3. Thiel, R.; Smith, M.E. State of the practice review of heap leach pad design issues. *Geotext. Geomembr.* **2004**, *22*, 555–568. [CrossRef]
4. Lupo, J.F.; Morrison, K.F. Geosynthetic design and construction approaches in the mining industry. *Geotext. Geomembr.* **2007**, *25*, 96–108. [CrossRef]
5. Touze-Foltz, N.; Lupo, J.; Barroso, M. Geoenvironmental applications of geosynthetics. Keynote Lecture. *Proc. Eurogeo* **2008**, *4*, 98.
6. Scheirs, J. *A Guide to Polymeric Geomembranes: A Practical Approach*; John Wiley & Sons: Hoboken, NJ, USA, 2009.
7. Rowe, R.K.; Hosney, M.S. Laboratory investigation of GCL performance for covering arsenic contaminated mine wastes. *Geotext. Geomembr.* **2013**, *39*, 63–77. [CrossRef]
8. Rowe, R.K.; Brachman, R.W.I.; Irfan, H.; Smith, M.E.; Thiel, R. Effect of underliner on geomembrane strains in heap leach applications. *Geotext. Geomembr.* **2013**, *40*, 37–47. [CrossRef]
9. Touze, N. Healing the world: A geosynthetics solution. *Geosynth. Int.* **2021**, *28*, 1–31. [CrossRef]
10. Rowe, R.K. Protecting the Environment with Geosynthetics: 53rd Karl Terzaghi Lecture. *J. Geotech. Geoenviron. Eng.* **2020**, *146*, 04020081. [CrossRef]
11. Rowe, R.K.; Jefferis, S. Protecting the environment from contamination with barrier systems: Advances and challenges, State-of-the-Art Lecture. In Proceedings of the 20th International Conference on Soil Mechanics and Geotechnical Engineering, Sydney, Australia, 1–5 May 2022; pp. 187–293.
12. Giroud, J.P.; Bonaparte, R. Leakage through liners constructed with geomembranes—Part I. Geomembrane liners. *Geotext. Geomembr.* **1989**, *8*, 27–67. [CrossRef]
13. Giroud, J.P.; Bonaparte, R. Leakage through liners constructed with geomembranes—Part II. Composite liners. *Geotext. Geomembr.* **1989**, *8*, 71–111. [CrossRef]
14. Rowe, R.K. Geosynthetics and the minimization of contaminant migration through barrier systems beneath solid waste. In Proceedings of the 6th International Conference on Geosynthetics, Atlanta, GA, USA, 25–29 March 1998; Volume 1, pp. 27–103.
15. Rowe, R.K. Long-term performance of contaminant barrier systems. *Geotechnique* **2005**, *55*, 631–678. [CrossRef]

16. Rowe, R.K. Short and long-term leakage through composite liners. *Can. Geotech. J.* **2012**, *49*, 141–169. [CrossRef]
17. Rowe, R.K. Geosynthetic clay liners: Perceptions and misconceptions. *Geotext. Geomembr.* **2020**, *48*, 137–156. [CrossRef]
18. Zhan, L.T.; Chen, C.; Bouazza, A.; Chen, Y.M. Evaluating leakages through GMB/GCL composite liners considering random hole distributions in wrinkle networks. *Geotext. Geomembr.* **2018**, *46*, 131–145. [CrossRef]
19. Pu, H.; Qiu, J.; Zhang, R.; Zheng, J. Assessment of consolidation-induced VOC transport for a GML/GCL/CCL composite liner system. *Geotext. Geomembr.* **2018**, *46*, 455–469. [CrossRef]
20. Chang, J.Y.; Feng, S.J.; Zheng, Q.T.; Shen, Y. Cyclic shear behavior of GMB/GCL composite liner. *Geotext. Geomembr.* **2021**, *49*, 593–603. [CrossRef]
21. Yan, H.; Wu, J.; Thomas, H.R.; Ding, H.; Zhan, L.; Xie, H. Analytical model for coupled consolidation and diffusion of organic contaminant transport in triple landfill liners. *Geotext. Geomembr.* **2021**, *49*, 489–499. [CrossRef]
22. Tang, L.; Francey, W.; Zheng, J.; Wang, X.; Luo, X. Filtration behaviour of staple fibre geotextiles under unequal biaxial tensile strains. *Geosynth. Int.* **2023**, 1–18. [CrossRef]
23. Fu, X.L.; Jiang, Z.Y.; Reddy, K.R.; Ruan, K.L.; Du, Y.J. Hydraulic conductivity, microstructure and compositional changes of sand-bentonite backfill in cutoff walls exposed to organic acids. *ASCE J. Geotech. Geoenviron. Eng.* **2023**, *149*, 04023060. [CrossRef]
24. Ng, C.W.W.; Chen, H.; Guo, H.; Chen, R.; Xue, Q. Life cycle analysis of common landfill final cover systems focusing on carbon neutrality. *Sci. Total Environ.* **2024**, *912*, 168863. [CrossRef] [PubMed]
25. Fan, J.Y.; Rowe, R.K. Effect of a lateral drainage layer on leakage through a defect in a geomembrane overlain by saturated tailings. *Geotext. Geomembr.* 2024; *in press*. [CrossRef]
26. Fan, J.Y.; Rowe, R.K. An empirical equation predicting the saturated hydraulic conductivity of tailings. *Can. Geotech. J.* 2024; *in press*. [CrossRef]
27. Rowe, R.K.; Quigley, R.M.; Brachman, R.W.I.; Booker, J.R. *Barrier Systems for Waste Disposal Facilities*; Taylor & Francis (E & FN Spon): London, UK, 2004.
28. Peggs, I.D.; Gassner, F.; Scheirs, J.; Tan, D.; Arango, A.M.N.; Burkard, B. Is there a resurgence of stress cracking in HDPE geomembranes. In Proceedings of the 10th International Geosynthetics Conference, Berlin, Germany, 21–25 September 2014; DGGT: Essen, Germany, 2014. CD-ROM.
29. Ewais, A.M.R.; Rowe, R.K.; Brachman, R.W.I.; Arnepalli, D.N. Service life of a high-density polyethylene geomembrane under simulated landfill conditions at 85° C. *J. Geotech. Geoenviron. Eng.* **2014**, *140*, 04014060. [CrossRef]
30. Rowe, R.K.; Shoaib, M. Long-term performance of high-density polyethylene (HDPE) geomembrane seams in municipal solid waste (MSW) leachate. *Can. Geotech. J.* **2017**, *54*, 1623–1636. [CrossRef]
31. Rowe, R.K.; Shoaib, M. Durability of HDPE geomembrane seams immersed in brine for three years. *J. Geotech. Geoenviron. Eng.* **2018**, *144*, 04017114. [CrossRef]
32. Badu-Tweneboah, K.; Giroud, J.P. Discussion of "Leakage through Holes in Geomembranes below Saturated Tailings" by R. Kerry Rowe, Prabeen Joshi, RWI Brachman, and H. McLeod. *J. Geotech. Geoenviron. Eng.* **2018**, *144*, 07018001. [CrossRef]
33. Eldesouky, H.M.G.; Brachman, R.W.I. Calculating local geomembrane strains from a single gravel particle with thin plate theory. *Geotext. Geomembr.* **2018**, *46*, 101–110. [CrossRef]
34. Brachman, R.W.I.; Joshi, P.; Rowe, R.K. A new laboratory apparatus for measuring leakage through geomembrane holes beneath mine tailings. *Can. Geotech. J.* **2017**, *54*, 147–157. [CrossRef]
35. Fan, J.Y.; Rowe, R.K. Effect of geosynthetic component characteristics on the potential for GCL internal erosion. *Geotext. Geomembr.* **2023**, *51*, 85–94. [CrossRef]
36. Fan, J.Y.; Rowe, R.K.; Brachman, R.W.I. Compressibility and permeability of sand-silt tailings mixtures. *Can. Geotech. J.* **2022**, *59*, 1348–1357. [CrossRef]
37. Fan, J.Y.; Rowe, R.K. Seepage through a circular geomembrane hole when covered by fine-grained tailings under filter incompatible conditions. *Can. Geotech. J.* **2022**, *59*, 410–423. [CrossRef]
38. Rowe, R.K.; Fan, J.Y. Effect of geomembrane hole geometry on leakage overlain by saturated tailings. *Geotext. Geomembr.* **2021**, *49*, 1506–1518. [CrossRef]
39. Rowe, R.K.; Fan, J.Y. A general solution for leakage through geomembrane defects overlain by saturated tailings and underlain by highly permeable subgrade. *Geotext. Geomembr.* **2022**, *50*, 694–707. [CrossRef]
40. Fan, J.Y.; Rowe, R.K. Leakage through a circular geomembrane hole overlain and underlain by silty sand tailings. *Geosynth. Int.* **2023**, 1–12. [CrossRef]
41. Fan, J.Y.; Rowe, R.K. Piping of silty sand tailings through a circular geomembrane hole. *Geotext. Geomembr.* **2022**, *50*, 183–196. [CrossRef]
42. Fan, J.Y.; Rowe, R.K. Effect of subgrade on leakage through a defective geomembrane seam below saturated tailing. *Geotext. Geomembr.* **2023**, *51*, 360–369. [CrossRef]
43. Fan, J.Y.; Rowe, R.K. Effect of subgrade on tensile strains in a geomembrane for tailings storage applications. *Can. Geotech. J.* **2023**, *60*, 18–30. [CrossRef]
44. Fan, J.Y.; Rowe, R.K. Effect of a soluble subgrade on leakage through a geomembrane defect. *Geosynth. Int.* **2023**, 1–13. [CrossRef]
45. Kenney, T.C.; Lau, D. Internal stability of granular filters. *Can. Geotech. J.* **1985**, *22*, 215–225. [CrossRef]
46. Rowe, R.K.; Joshi, P.; Brachman, R.W.I.; McLeod, H. Leakage through holes in geomembranes below saturated tailings. *J. Geotech. Geoenviron. Eng.* **2017**, *143*, 04016099. [CrossRef]

47. Fan, J.Y.; Rowe, R.K. Effect of tailings fines content on leakage though circular geomembrane holes overlain by saturated tailings. In *Geosynthetics: Leading the Way to a Resilient Planet*; CRC Press: Boca Raton, FL, USA, 2023; pp. 1643–1649.
48. Taylor, D. *Fundamentals of Soil Mechanics*; Chapman and Hall, Limited: New York, NY, USA, 1948.
49. Chou, Y.C.; Brachman, R.W.; Rowe, R.K. Leakage through a hole in a geomembrane beneath a fine-grained tailings. *Can. Geotech. J.* **2022**, *59*, 372–383. [CrossRef]
50. Sherard, J.L.; Dunnigan, L.P.; Talbot, J.R. Basic properties of sand and gravel filters. *J. Geotech. Eng.* **1984**, *110*, 684–700. [CrossRef]
51. Foster, M.; Fell, R. Assessing embankment dam filters that do not satisfy design criteria. *J. Geotech. Geoenviron. Eng.* **2001**, *127*, 398–407. [CrossRef]
52. Wong, R.C.; Mills, B.N.; Liu, Y.B. Mechanistic model for one-dimensional consolidation behavior of nonsegregating oil sands tailings. *J. Geotech. Geoenviron. Eng.* **2008**, *134*, 195–202. [CrossRef]
53. Fell, R.; Wan, C.F.; Cyganiewicz, J.; Foster, M. Time for development of internal erosion and piping in embankment dams. *J. Geotech. Geoenviron. Eng.* **2003**, *129*, 307–314. [CrossRef]
54. Rollin, A.L.; Marcotte, M.; Jacqueline, T.; Chaput, L. Leak location in exposed geomembrane liners using an electrical leak detection technique. In Proceedings of the Geosynthetic'99, Industrial Fabrics Association International, Boston, MA, USA, 28–30 April 1999; IFAI: Roseville, MI, USA, 1999; Volume 2, pp. 615–626.
55. Gilson-Beck, A. Controlling leakage through installed geomembranes using electrical leak location. *Geotext. Geomembr.* **2019**, *47*, 697–710. [CrossRef]
56. Gilson-Beck, A.; Giroud, J.P. A quantification of the short-term reliability of HDPE geomembrane seaming methods. *Geosynth. Int.* **2022**, *29*, 337–341. [CrossRef]
57. Zhang, L.; Bouazza, A.; Rowe, R.K.; Scheirs, J. Effect of welding parameters on properties of HDPE geomembrane seams. *Geosynth. Int.* **2017**, *24*, 408–418. [CrossRef]
58. Rowe, R.K.; Ali, M.M. Effect of welding parameters on properties of HDPE geomembrane extrusion welds. *Geotext. Geomembr.* **2024**, *52*, 355–367. [CrossRef]
59. Ali, M.; Rowe, R.K. Long-term performance of HDPE extrusion Welds aged at 85 °C in synthetic leachate. *Geosynth. Int.* **2024**, 1–37. [CrossRef]
60. Giroud, J.; Tisseau, B.; Soderman, K.; Beech, J. Analysis of strain concentration next to geomembrane seams. *Geosynth. Int.* **1995**, *2*, 1049–1097. [CrossRef]
61. Kavazanjian, E.; Andresen, J.; Gutierrez, A. Experimental evaluation of HDPE geomembrane seam strain concentrations. *Geosynth. Int.* **2017**, *24*, 333–342. [CrossRef]
62. Cheng, Q.; Tang, C.S.; Zeng, H.; Zhu, C.; An, N.; Shi, B. Effects of microstructure on desiccation cracking of a compacted soil. *Eng. Geol.* **2020**, *265*, 105418. [CrossRef]
63. Tang, C.S.; Zhu, C.; Cheng, Q.; Zeng, H.; Xu, J.J.; Tian, B.G.; Shi, B. Desiccation cracking of soils: A review of investigation approaches, underlying mechanisms, and influencing factors. *Earth-Sci. Rev.* **2021**, *216*, 103586. [CrossRef]
64. Tognon, A.R.; Rowe, R.K.; Moore, I.D. Geomembrane strain observed in large-scale testing of protection layers. *J. Geotech. Geoenviron. Eng.* **2000**, *126*, 1194–1208. [CrossRef]
65. Marcotte, B.A.; Fleming, I.R. The role of undrained clay soil subgrade properties in controlling deformations in geomembranes. *Geotext. Geomembr.* **2019**, *47*, 327–335. [CrossRef]
66. Rowe, R.K.; Yu, Y. Magnitude and significance of tensile strains in geomembrane landfill liners. *Geotext. Geomembr.* **2019**, *47*, 439–458. [CrossRef]
67. Rowe, R.K.; Abdelaal, F.B. Antioxidant depletion in HDPE Geomembrane with HALS in low pH heap leach environment. *Can. Geotech. J.* **2016**, *53*, 1612–1627. [CrossRef]
68. Abdelaal, F.B.; Kerry Rowe, R. Effect of high pH found in low-level radioactive waste leachates on the antioxidant depletion of a HDPE geomembrane. *J. Hazard. Toxic Radioact. Waste* **2017**, *21*, D4015001. [CrossRef]
69. Abdelaal, F.B.; Samea, A. Chemical durability of elastomeric bituminous geomembranes (BGMs) in heap leach pad applications. *Geosynth. Int.* **2023**, 1–18. [CrossRef]
70. Abdelaal, F.B.; Samea, A. The long-term performance of an elastomeric bituminous geomembrane (BGM) under single-sided conditions. *Can. Geotech. J.* 2023; *in press*. [CrossRef]
71. Abdelaal, F.B.; Rowe, R.K.; Morsy, M.S.; e Silva, R.A. Degradation of HDPE, LLDPE, and blended polyethylene geomembranes in extremely low and high pH mining solutions at 85 °C. *Geotext. Geomembr.* **2023**, *51*, 27–38. [CrossRef]
72. Rowe, R.K.; Abdelaal, F.B.; Zafari, M.; Morsy, M.S.; Priyanto, D.G. An approach to high-density polyethylene (HDPE) geomembrane selection for challenging design requirements. *Can. Geotech. J.* **2020**, *57*, 1550–1565. [CrossRef]
73. Francey, W.; Rowe, R.K. Factors affecting the tensile strength of bituminous geomembrane seams. *Geosynth. Int.* **2024**, 1–25. [CrossRef]
74. Rowe, R.K.; Morsy, M.S.; Ewais, A.M.R. Representative stress crack resistance of polyolefin geomembranes used in waste management. *Waste Manag.* **2019**, *100*, 18–27. [CrossRef]
75. Touze-Foltz, N.; Farcas, F. Long-term performance and binder chemical structure evolution of elastomeric bituminous geomembranes. *Geotext. Geomembr.* **2017**, *45*, 121–130. [CrossRef]
76. Samea, A.; Abdelaal, F.B. Effect of elevated temperatures on the degradation behaviour of elastomeric bituminous geomembranes. *Geotext. Geomembr.* **2023**, *51*, 219–232. [CrossRef]

77. Samea, A.; Abdelaal, F.B. Durability of two bituminous geomembranes (BGMs) with different thicknesses in MSW synthetic leachate. *Waste Manag.* **2023**, *165*, 179–188. [CrossRef] [PubMed]
78. Addis, P.; Andruchow, B.; Wislesky, I. Bituminous Geomembrane Failure at a Co-Disposal Tailings Storage Facility. In Proceedings of the Tailings and Mine Waste, Banff, AB, Canada, 2–5 October 2016.
79. Bremner, H.; Belanger, J.-F.; Charpentier, C.; Jacquelin, T. Case study on quality control and leak location performed on a bituminous liner mine closure project near the arctic circle in NWT, Canada. In Proceedings of the GeoAmericas—Pan-American Conference on Geosynthetics, Miami Beach, FL, USA, 10–13 April 2016.